CLOUD COVER AND HORIZONTAL PLANE EYE DAMAGING SOLAR UV EXPOSURES

Parisi, A.V[a,#]., Downs, N[a]

[a]Centre for Astronomy, Solar Radiation and Climate, University of Southern Queensland, Toowoomba, 4350, Australia. Ph: 61 7 4631 2226. FAX: 61 7 4631 2721. Email: parisi@usq.edu.au

[#]To whom correspondence should be addressed.

Abstract

The spectral UV and the cloud cover were measured at intervals of five minutes with an integrated cloud and spectral UV measurement system at a sub-tropical Southern Hemisphere site for a six month period and solar zenith angle (SZA) range of 4.7^{o} to approximately 80^{o}. The solar UV spectra were recorded between 280 and 400 nm in 0.5 nm increments and weighted with the action spectra for photokeratitis and cataracts in order to investigate the effect of cloud cover on the horizontal plane biologically damaging UV irradiances for cataracts (UVBE$_{cat}$) and photokeratitis (UVBE$_{pker}$). Eighty five percent of the recorded spectra produced a measured irradiance to a cloud free irradiance ratio of 0.6 and higher while 76% produced a ratio of 0.8 and higher. Empirical non-linear expressions as a function of SZA have been developed for all sky conditions to allow the evaluation of the biologically damaging UV irradiances for photokeratitis and cataracts from a knowledge of the unweighted UV irradiances.

Keywords: Ultraviolet; cloud; cataract; photokeratitis, spectral

Introduction

The major cause of variation in the solar ultraviolet (UV) radiation at a given location for a fixed solar elevation angle is the presence of clouds (Sabburg 2000; Bodeker and McKenzie 1996). Clouds may even at times increase the UV above that on a cloud-free day (Estupinan *et al* 1996; Sabburg *et al* 2001; Sabburg *et al* 2003; Sabburg and Wong 2000a). The effect of cloud has been reported to be dependent on wavelength and solar zenith angle (SZA). Seckmeyer *et al* (1996) reported a higher transmittance of clouds in the UVB (280-320 nm) compared to the UVA (320-400 nm) waveband. For the cases when the sun is covered by cloud, the global solar radiation from 300 to 3,000 nm is reduced more than the UVA and UVB irradiances (Blumthaler *et al* 1994). Nemeth *et al* (1996) reported an increase in UVB transmission for a SZA greater than 60^o compared to a SZA of less than 60^o due to increased reflection by cloud edges. For the cases where the UV has been increased above that of a cloud-free day, the increase has been reported to be approximately wavelength independent for wavelengths longer than 306 nm with a generally increasing wavelength dependency for shorter wavelengths (Sabburg *et al* 2003).

Previous research has reported on models to predict the global erythemal UV based on the cloud amount and cloud type (for example, Thiel *et al* 1997). Models have been developed for evaluating the global UVB based on a range of cloud parameters (Sabburg and Wong 2000b) and the diffuse solar UVA and UVB for partly cloudy skies (Grant and Gao 2003). The ratio of the measured photosynthetically active photon flux density (PPFD) to calculated cloud-free sky PPFD at the same sun angle has been employed to estimate the normalized UVB irradiances (Grant and Heisler 2000). Global solar radiation irradiances averaged over 10 min periods from a

pyranometer have been found to have a stronger correlation with UV irradiances than either satellite or ground based cloud observations (McKenzie *et al* 1998).

Personal solar UV exposure is due to sunlight received as both direct radiation and diffuse radiation in both full sun and shade (Parisi and Kimlin 1999a; 1999b; Parisi *et al* 2000; Sliney 1986, 1994). The diffuse component is the sunlight that has been scattered and reflected by the atmosphere and the environment. The diffuse component of the solar UV at a sub-tropical latitude and averaged over each season has been measured for SZA's of 4^o to 70^o to range from 23 to 59% in full sun and 58 to 71% in tree shade (Parisi *et al* 2001). The maximum value of the diffuse fraction recorded in this research was as high as 100%. Grant and Gao (2003) measured the clear sky diffuse UVB to range from 40% to 70% for SZA of 15^o and range to 100% for SZA of 75^o. The diffuse component of UV can be increased by cloud due to reflection from cloud edges and can constitute a significant contribution of the UV exposure to human eyes and skin. Diffuse UV is incident from all directions, difficult to minimise with the usage of hats, tree shade and shade structures and accompanied under cloud by the possible increase in exposure time because of lower temperatures. Consequently, a significant component of the UV exposure to humans' skin and eyes is due to UV radiation under cloudy or partially cloudy skies.

Sun-related eye disorders are potentially preventable diseases. A range of eye disorders including, cataracts, age-related macular degeneration, pterygium and photokeratitis have been shown to be sun-related (Young 1994). Cataracts are a major public health problem, being the primary cause of blindness in humans (West *et al* 1998). The variation of the daily biologically effective UV through the year depends

on the relative response of the particular action spectrum (Parisi *et al* 2003). The dependence of the spectral UV weighted with different action spectra has been investigated for changes in altitude (Ambach *et al* 1993) and orientation of the receiver plane (Parisi and Kimlin, 1999a) and for different shade settings (Turnbull and Parisi, 2003). The goal of this research was to determine the effect of cloud on the biologically damaging UV for cataracts ($UVBE_{cat}$) and photokeratitis ($UVBE_{pker}$) for the range of SZA encountered at a Southern Hemisphere sub-tropical site and develop a relationship between $UVBE_{cat}$ and $UVBE_{pker}$ compared to the broadband UV for all sky conditions encountered over a six month period.

Materials and Methods

Spectral Equipment

In order to calculate the biologically damaging UV for cataracts and photokeratitis, the spectral solar UV was recorded with a UV spectroradiometer (Figure 1) on an unshaded roof at a sub-tropical latitude in Toowoomba, (27.5 ^{o}S, 693 m above sea level) Australia. This site has a relatively unpolluted atmosphere. The spectroradiometer (model DTM300, Bentham Instruments, Reading, UK) is based on a double grating monochromator with a pair of holographic gratings with 2400 lines/mm blazed at 250 nm and with a 600 mm focal length (model DTMc300F), a UV sensitive detector comprising of a side window photomultiplier tube with a bialkali photocathode (model DH10), amplifier with software variable gain (model 267) and integrating analogue to digital converter with 100 ms integration period (model 228A). Solar radiation enters the spectroradiometer via the input optics (Figure 1) provided by a diffuser (model D5-H) and connected by a one metre long, 4 mm diameter optical fibre to the input slit of the monochromator. Input and output slit

widths of 0.37 mm are employed on the monochromator to provide a bandwidth of 0.5 nm as specified by the manufacturer.

The instrument is installed in an environmentally sealed container that is attached to the roof, the optic fibre enters the container through the side. The manufacturer has determined the error associated with the cosine response of the diffuser as less than ±0.8% for a SZA up to 70^o. For an SZA of 80^o, the cosine error is 3.3%. The dark count error is subtracted by the spectroradiometer software for each scan. The maximum variability of the dark count about the mean dark count was ±0.1% over the temperature range of 5 to 24 ^oC. Temperatures inside the container are software recorded every 5 minutes at the time of a scan. The instrument is currently not temperature stabilised, however it is intended to be temperature stabilised in the near future. In the meantime, the manufacturer supplied temperature coefficients of -0.4% /^oC have been applied to temperature correct the data employed in this research.

On each day, the spectroradiometer is scheduled to start scanning at dawn (5:00 am local time), and thereafter every 5 minutes till dusk (7:00 pm local time) from 280 to 400 nm in increments of 0.5 nm. Prior to each scan, the dark current is measured. Each scan is initialised at 60 seconds before the five minute point with the collection of the spectrum starting at approximately the five minute point and the entire process taking approximately three minutes. Data from the instrument is provided in IEEE format to a computer in the laboratory at a distance of approximately 80 m. GPIB extenders (model GPIB-130, National Instruments Australia) are utilised at the instrument and computer ends of the communication line to allow transmission of the data over this distance. The spectroradiometer control, data acquisition, display and

manipulation is performed by the BenWin+ software (Bentham Instruments, Reading, UK).

The data set employed in this paper uses the UV spectra recorded at five minute intervals from 1 January 2003 to 30 June 2003. Over this period, the monthly averages of the daily ozone column thickness over the site, measured by the Total Ozone Mapping Spectrometer (TOMS) ranged from 263 to 276 DU (Dobson Units). The TOMS web site (http://toms.gsfc.nasa.gov/ozone/ozone.html) was employed to obtain this data. For this period, the instrument was irradiance calibrated on 17 March 2003 against a 150 W quartz tungsten halogen (QTH) lamp calibrated to the National Physical Laboratory, UK standard and wavelength calibrated against the UV spectral lines of a mercury lamp. There was a ±3% error associated with this calibration due to irradiance and lamp traceability errors. On a 14 to 30 day basis, the instrument was checked for irradiance stability using three sets of 150 W QTH lamps and the spectral lines of a mercury lamp were also employed for wavelength calibration. These checks were performed on-site with the lamps in a light tight housing that mounted directly onto the input optics of the instrument. The error due to wavelength variation was of the order of ±1.1% and the variation of the stability of the spectroradiometer output was 5.2% as determined by the change in the measured output of the lamps employed in checking the stability of the spectroradiometer. The overall absolute irradiance accuracy of the Bentham spectroradiometer was of the order of ±9% based on the temporal stability, cosine error, dark count variability and the traceability of the absolute irradiance of the calibration lamps.

Biologically Damaging UV

For a particular action spectrum, A(λ), the biologically damaging UV irradiance, UVBE, is calculated employing:

$$UVBE = \int_{UV} S(\lambda)A(\lambda)d\lambda \qquad (1)$$

where S(λ) is the measured spectral irradiance and dλ is the wavelength increment of the spectral data, 0.5 nm in this case. Practically, the integration is replaced by the summation over the UV waveband and dλ by Δλ. To calculate the broadband unweighted UV, the function A(λ) is replaced by 1 and the summation undertaken from 295 to 400 nm. In this research, the action spectra for photokeratitis (CIE 1986) and cataracts (Oriowo *et al* 2001) as shown in Figure 2 and Figure 3 have been employed. The respective action spectra have been linearly interpolated between the data points to 0.5 nm. The cataract action spectrum is for in- vitro cataract formation for a cultured porcine lens. The pig's lens is similar in shape and size to the human lens and as a result inferences may be made to the lens of humans (Oriowo *et al* 2001).

Cloud Measurements

The amount of cloud cover was quantified with a Total Sky Imager (TSI) (model TSI-440, Yankee Environmental Systems, MA, USA) currently installed on a building roof at the University at a distance of approximately five metres from the spectroradiometer. It is configured to automatically collect data every five minutes for SZA less than 80^o and is connected via a 10Base-T ethernet port to a local area network. The images are recorded on a networked computer that is the same one controlling the spectroradiometer. Along with the spectroradiometer, it forms a synchronized integrated automatic cloud and spectral UV measurement system.

A CCD camera and software package capture 352 x 288 pixel, 24 bit, colour images into JPEG format data files, which are then analysed for fractional cloud cover. The operation of the instrument is based on a hemispherical reflective dome that points upwards on a horizontal plane. An image of the sky and clouds that is reflected on this dome is captured by a CCD camera that is suspended above and over the centre of the dome by a thin arm support. Almost all of the sky is imaged and the analysis for cloud cover is performed on the image within a 160^{o} field of view. The portion of the sky near the horizon in the part of the image that is not analysed relates to approximately 12.5% of the sky. In order to prevent reflection of the sun and consequently possibly damage to the CCD camera, a black shadow band is taped onto the reflective dome and the dome rotates to track the sun across the sky throughout the day using a software based almanac. This shadow band corresponds to approximately 9% of the image. The system provides the cloud cover reading for both thin cloud and opaque cloud by subtracting the blue light level from the red light level in each image at a user-defined interval, currently 5 minutes, eliminating the issue of subjectivity. The error in the cloud cover algorithm has not been estimated due to variation with cloud type and the subjectivity in human visual observations. Additionally, the TSI software provides the SZA at the time that each image is recorded. This was recorded with the fractional amount of cloud cover and employed in the analysis of the data as a function of SZA.

The amount of cloud cover at the time of each spectral scan was employed to determine the spectral scans that were collected for relatively cloud free skies. A criterion of less than 2% cloud recorded by the TSI was employed to classify the scan

as being cloud free. As the TSI image is recorded at the start of the two minute spectroradiometer scan, there is the possibility that the amount of cloud cover can change over this period. However, in this paper, the TSI was employed to establish the cloud free scans and it is assumed that there would be only a minimal increase from less than 2% cloud cover over this period.

Results

UVBE Variability

The variation of the spectral $UVBE_{pker}$ and $UVBE_{cat}$ for three different SZAs at cloud free periods for photokeratitis and cataracts is provided in Figure 2 and Figure 3. The SZAs were 6^o, 51^o and 71^o and corresponded to 12:15 EST, 6 January, noon, 10 June and 8:00 EST, 10 June respectively. Additionally for the $UVBE_{pker}$, an example of the effect of cloud on the UVBE is shown for a SZA of 51^o. The spectral UVBE end at 316 nm and 365 nm for $UVBE_{pker}$ and $UVBE_{cat}$ respectively as that is the longer wavelength limit of the action spectra. The peak UVBE and the short wavelength cutoff, shift to the shorter wavelengths with decreasing SZA. The difference between the spectral UVBE for the different SZAs is less at the longer wavelengths compared to the wavelengths where the peak UVBE occurs.

The solar UV spectra collected at the times when both the spectroradiometer and TSI were operational have been employed to calculate the $UVBE_{pker}$ and $UVBE_{cat}$ irradiances shown in Figure 4 and Figure 5. This corresponds to 12,449 solar UV spectra over the six month period corresponding to the times over this period when both the TSI and spectroradiometer were operational. From this set, 1,998 spectra have been classified as being collected during cloud free periods. These were

employed to calculate the $UVBE_{pker}$ and $UVBE_{cat}$ irradiances shown in part (a) of Figure 4 and Figure 5. The maximum $UVBE_{pker}$ and $UVBE_{cat}$ irradiances were 306 and 479 mW m^{-2} respectively. The regression curve fitted to each data set with the SPSS version 11.5 package for the cloud free cases is for photokeratitis:

$$UVBE_{p\,\mathrm{ker}} = 244.76 + 0.7575SZA - 0.1401SZA^2 + 0.001167SZA^3 \text{ mW m}^{-2} \quad (2)$$

with an R^2 of 0.99. Similarly, for cataracts, the cloud free envelope is:

$$UVBE_{cat} = 382.40 + 1.605SZA - 0.2236SZA^2 + 0.001822SZA^3 \text{ mW m}^{-2} \quad (3)$$

with an R^2 of 0.99.

The cloud free envelopes produce a maximum and minimum $UVBE_{pker}$ of 245 and 6.5 mW m^{-2} for the SZA range of 5^o to 80^o respectively. Similarly, the corresponding values are 385 and 12.4 mW m^{-2} for $UVBE_{cat}$. The single error bar for an SZA of 5^o on each graph represents the 95^{th} percentile of the values classified as cloud free and is ±14.2 mW m^{-2} and ±23.1 mW m^{-2} for $UVBE_{pker}$ and $UVBE_{cat}$ respectively. Factors influencing this variation about the fitted curve for the cloud free cases are changes in the atmospheric conditions such as ozone and aerosol concentrations over the six months of the data collection period, along with the ±6% uncertainty of the spectral irradiance measurements based on the cosine error and the temporal stability of the spectroradiometer.

The measured $UVBE_{cat}$ was compared to the cloud free regression curve for the appropriate SZA. The ratios were categorized by cloud cover fraction shown in Figure 6 and the number expressed as a percentage of the total number of cases. The cloud free column is the percentage of values within ±23.1 mW m^{-2} (95^{th} percentile) of the cloud free regression curve. The > 1 column is the percentage of values higher than

the cloud free case and represents the cases where the UVBE has been enhanced by cloud above that of the cloud free case (Parisi and Downs, 2004). The upper limit of the cloud free case employed in calculating this column was taken as the value of the regression curve at the appropriate SZA plus the 95^{th} percentile. The columns to the right of the cloud free case represent the percentage of values less than the cloud free case. In this case the lower limit of the cloud free case that was employed in the calculation was taken as the value of the regression curve at the appropriate SZA minus the 95^{th} percentile.

Relationships between $UVBE_{pker}$, $UVBE_{cat}$ and UV

The ratios of the $UVBE_{cat}$ to $UVBE_{pker}$ for all sky conditions is provided in Figure 7. This is non-linear and increases for the larger SZA. This is due to the increase in the ratio of UVA to UVB irradiances for larger SZAs (Kimlin *et al* 2002) and the cataract action spectrum possessing a response in the UVA waveband compared to no response in the UVA for the photokeratitis action spectrum.

In order to determine empirical expressions to allow evaluation of the $UVBE_{pker}$ and $UVBE_{cat}$ from the broadband UV for all sky conditions, the ratio of the biologically damaging UV irradiances for photokeratitis and cataracts to the unweighted UV is shown in Figure 8. The ratios are non-linear and decrease for the larger SZA. This is due to the combined effect of the increase in the ratio of UVA to UVB irradiances for larger SZAs and the lower effectiveness of the two action spectra at the longer wavelengths. Additionally, the relationship is different for the two ratios. The $UVBE_{cat}$/UV is higher than the $UVBE_{pker}$/UV ratio due to the photokeratitis action spectrum not having any influence for wavelengths longer than 316 nm, whereas the cataract action spectrum extends into the UVA wavelengths.

Regression curves (Figure 8) were fitted to the ratios with the SPSS version 11.5 package and are as follows:

$$\frac{UVBE_{p\,\mathrm{ker}}}{UV} = 0.00343 - 1.145\times10^{-5}\,SZA - 3.577\times10^{-7}\,SZA^2 \qquad (4)$$

with an R^2 of 0.88.

$$\frac{UVBE_{cat}}{UV} = 0.00534 - 1.222\times10^{-5}\,SZA - 5.738\times10^{-7}\,SZA^2 \qquad (5)$$

with an R^2 of 0.87. These empirical expressions allow the evaluation of the $UVBE_{pker}$ and $UVBE_{cat}$ irradiances from a knowledge of the unweighted UV irradiances for all sky conditions.

Discussion

This paper has investigated the influence of cloud on the biologically damaging UV for sun-related eye disorders and whether a strong relationship is available between the biologically damaging UV for photokeratitis and cataracts and the unweighted UV for all sky conditions. The spectral UV and the cloud cover were measured at intervals of five minutes with an integrated cloud and spectral UV measurement system at a sub-tropical Southern Hemisphere site during a six month period. The data covered the SZA range of 4.7^o to approximately 80^o. Previous research has reported spectral UV measurements at intervals of 5^o of SZA (McKenzie *et al* 1992; Bodhaine *et al* 1997) and the broadband UV and cloud properties at six minute intervals (Sabburg and Wong 2000b). To the authors' knowledge, the data set in this paper is the first reported that has recorded five minute spectral UV and cloud cover concurrently over an extended period of time.

The extensive data set has allowed the investigation of the effect of cloud on the biologically damaging UV for photokeratitis and cataracts. Eighty five percent of the recorded spectra produced a measured irradiance to a cloud free irradiance ratio of 0.6 or higher while 76% produced a ratio of 0.8 and higher. Empirical expressions have been developed for all sky conditions to allow the evaluation of the $UVBE_{pker}$ and $UVBE_{cat}$ irradiances from a knowledge of the unweighted UV irradiances. These expressions are a function of SZA. There is good correlation between these two sets of biologically damaging UV and the broadband UV. Generally, unweighted UV is monitored and recorded with broadband instruments at more locations than the biologically damaging UV for sun-related eye problems. The regression equations developed in this research allow the evaluation of the $UVBE_{pker}$ and $UVBE_{cat}$ irradiances from a knowledge of the unweighted UV. The empirical expressions are expected to apply for the SZA range of 4.7^{o} to approximately 80^{o} for sub-tropical latitudes and temperate latitudes. However, they may not necessarily apply in tropical latitudes where the vertical extent of clouds may at times be different.

***Acknowledgements*:**

The authors acknowledge Dr Jeff Sabburg and the technical staff in Physics and the Sciences workshop, USQ for their assistance in this project, along with the funding provided by the Australian Research Council for the spectroradiometer and the University of Southern Queensland for the TSI.

References

Ambach W, Blumthaler M, Schopf T (1993) Increase of biologically effective ultraviolet radiation with altitude. J Wild Med 4:189-197

CIE (International Commission on Illumination) (1986) Photokeratitis. CIE J 5:19-23

Blumthaler M, Ambach W, Salzgeber M (1994) Effects of cloudiness on global and diffuse UV irradiance in a high-mountain area. Theor Appl Climatol 50:23-30

Bodeker GE, McKenzie RL (1996) An algorithm for inferring surface UV irradiance including cloud effects. J Appl Meteorol 35:1860-1877

Bodhaine BA, Dutton EG, Hofmann DJ, Mckenzie RL, Johnston PV (1997) UV measurements at Mauna Loa: July 1995 to July 1996. J Geophys Res 102:19265-19273

Estupinan JG, Raman S, Crescenti GH, Streicher JJ, Barnard WF (1996) Effects of cloud and haze on UV-B radiation. J Geophys Res 104:16807-16816

Kimlin MG, Parisi AV, Sabburg J, Downs ND (2002) Understanding the UVA environment at a sub-tropical site and its consequent impact on human UVA exposure. Photochem Photobiol Sci 1:478-482

Grant RH, Gao W (2003) Diffuse fraction of UV radiation under partly cloudy skies as defined by the Automated Surface Observation System (ASOS). J Geophys Res 108(D2):4046, doi:10.1029/2002JD002201

Grant RH, Heisler GM (2000) Estimation of ultraviolet-B irradiance under variable cloud conditions. J Appl Met 39:904-916

McKenzie RL, Johnston PV, Kotkamp M, Bittar A, Hamlin JD (1992) Solar ultraviolet spectroradiometry in New Zealand: instrumentation and sample results from 1990. Appl Optics 31:6501-6509

McKenzie RL, Paulin KJ, Bodeker GE, Liley JB (1998) Cloud cover measured by satellite and from the ground: relationship to UV radiation at the surface. Int J Remote Sensing 19:2969-2985

Nemeth P, Toth Z, Nagy Z (1996) Effect of weather conditions on UV-B radiation reaching the earth's surface. J Photochem Photobiol B: Biol 32:177-181

Oriowo OM, Cullen AP, Chou BR, Sivak JG (2001) Action spectrum and recovery for in vitro UV-induced cataract using whole lenses. Invest Ophthal Vis Sci 42:2596-2602

Parisi AV, Downs N (2004) Variation of the enhanced biologically damaging solar UV due to clouds. submitted Photchem Photobiol Sci

Parisi AV, Kimlin MG (1999a) Horizontal and sun normal spectral biologically effective ultraviolet irradiances. J Photochem Photobiol B: Biol 53:70-74

Parisi AV, Kimlin MG (1999b) Comparison of the spectral biologically effective solar ultraviolet in adjacent tree shade and sun. Phys Med Biol 44:2071-2080

Parisi AV, Green A, Kimlin MG (2001) Diffuse solar ultraviolet radiation and implications for preventing human eye damage. Photochem Photobiol 73:135-139

Parisi AV, Kimlin MG, Wong JCF, Wilson M (2000) Diffuse component of the solar ultraviolet radiation in tree shade. J Photochem Photobiol B: Biol. 54:116-120

Parisi AV, Sabburg J, Kimlin MG (2003) Comparison of biologically damaging spectral solar ultraviolet radiation at a southern hemisphere sub-tropical site. Phys Med Biol 48:N121-N129

Sabburg J (2000) Quantification of Cloud around the Sun and its correlation to Global UV Measurement. *PhD thesis* Queensland University of Technology, Brisbane, Australia.

Sabburg J, Parisi AV, Wong J (2001) Effect of cloud on UVA and exposure to humans. Photochem Photobiol 74:412-416

Sabburg JM, Parisi AV, Kimlin MG (2003) Enhanced spectral UV irradiance: a one year preliminary study. Atmos Res 66:261-272

Sabburg J, Wong J (2000a) The effect of clouds on enhancing UVB irradiance at the earth's surface: a one year study. Geophys Res Lett 27:3337-3340

Sabburg J, Wong J (2000b) Evaluation of a sky/cloud formula for estimating UV-B irradiance under cloudy skies. J Geophys Res 105:29,685-29,691

Seckmeyer G, Erb R, Albold A (1996) Transmittance of a cloud is wavelength-dependent in the UV-range. Geophys Res Lett 23:2753-2755

Sliney DH (1986) Physical factors in cataractogenenesis: ambient ultraviolet radiation and temperature. Invest Ophthal Vis Sci 27:781-790

Sliney DH (1994) Epidemiological studies of sunlight and cataract: the critical factors of ultraviolet exposure geometry. Ophthal Epidemiol 1:107-119

Thiel S, Steiner K, Seidlitz HK (1997) Modification of global erythemally effective irradiance by clouds. Photochem Photobiol 65:969-973

Turnbull D, Parisi AV (2003) Spectral UV in Public Shade Settings. J Photochem. Photobiol B: Biol 69:13-19

West SK, Duncan DD, Munoz B, Rubin GS, Fried LP, Bandeen-Roche K, Schein OD (1998) Sunlight exposure and the risk of lens opacities in a population based study. J Am Med Assoc 280:714-718

Young RW (1994) The family of sunlight-related eye diseases. Opt Vision Sci 71:125-144

FIGURE CAPTIONS

Figure 1 - Spectroradiometer installed in the environmentally sealed container on an unshaded roof.

Figure 2 - $UVBE_{pker}$ at cloud free periods for SZA of 6^o (12:15 EST, 6 January, 2003), 51^o (12:00 EST, 10 June 2003) and 71^o (8:00 EST, 10 June 2003) and for a cloudy period with SZA of 51^o (11:35 EST, 30 June 2003). The action spectrum is plotted on the right hand axis.

Figure 3 - $UVBE_{cat}$ at cloud free periods for SZA of 6^o (12:15 EST, 6 January, 2003), 51^o (12:00 EST, 10 June 2003) and 71^o (8:00 EST, 10 June 2003). The action spectrum is plotted on the right hand axis.

Figure 4 - The $UVBE_{pker}$ for (a) cloud free conditions and (b) all sky conditions as a function of SZA. The error bar shown in part (a) represents the 95^{th} percentile of the cloud free cases.

Figure 5 - The $UVBE_{cat}$ for (a) cloud free conditions and (b) all sky conditions as a function of SZA. The error bar shown in part (a) represents the 95^{th} percentile of the cloud free cases.

Figure 6 – Percentages within each range of the measured/cloud free values for $UVBE_{cat}$. The cloud free column is the percentage of values within ±23.1 mW m^{-2} (95^{th} percentile) of the cloud free regression curve. The > 1 column is the percentage of values higher than the cloud free regression curve at the appropriate SZA plus the 95^{th} percentile. The other columns are the percentages less than the cloud free regression curve at the appropriate SZA minus the 95^{th} percentile.

Figure 7 – Ratio of the $UVBE_{cat}$ to $UVBE_{pker}$ irradiances for all sky conditions.

Figure 8 – Ratio of the biologically effective UV to the unweighted UV for (a) photokeratitis and (b) cataracts and the fitted regression curves.

Figure 1 - Spectroradiometer installed in the environmentally sealed container on an unshaded roof.

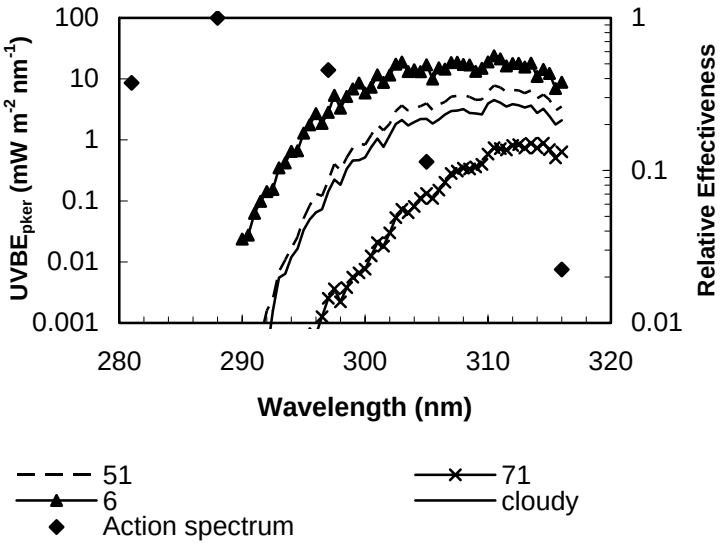

Figure 2 - UVBE$_{pker}$ at cloud free periods for SZA of 6^{o} (12:15 EST, 6 January, 2003), 51^{o} (12:00 EST, 10 June 2003) and 71^{o} (8:00 EST, 10 June 2003) and for a cloudy period with SZA of 51^{o} (11:35 EST, 30 June 2003). The action spectrum is plotted on the right hand axis.

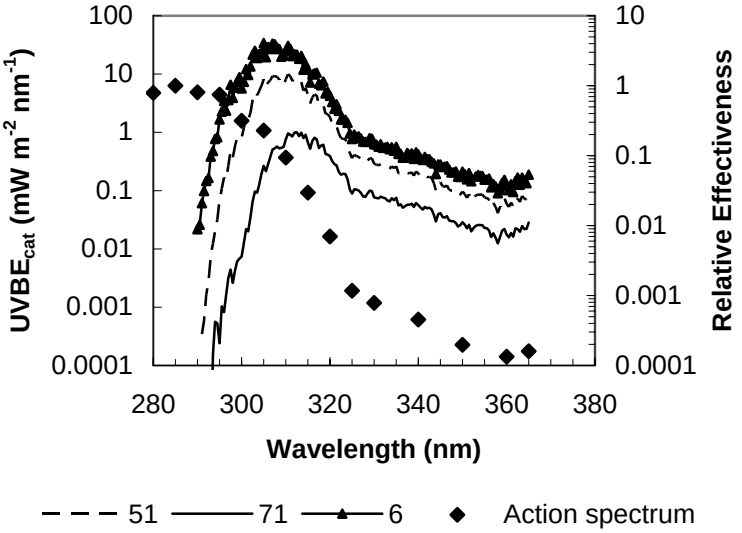

Figure 3 - UVBE$_{cat}$ at cloud free periods for SZA of 6^{o} (12:15 EST, 6 January, 2003), 51^{o} (12:00 EST, 10 June 2003) and 71^{o} (8:00 EST, 10 June 2003). The action spectrum is plotted on the right hand axis.

(a)

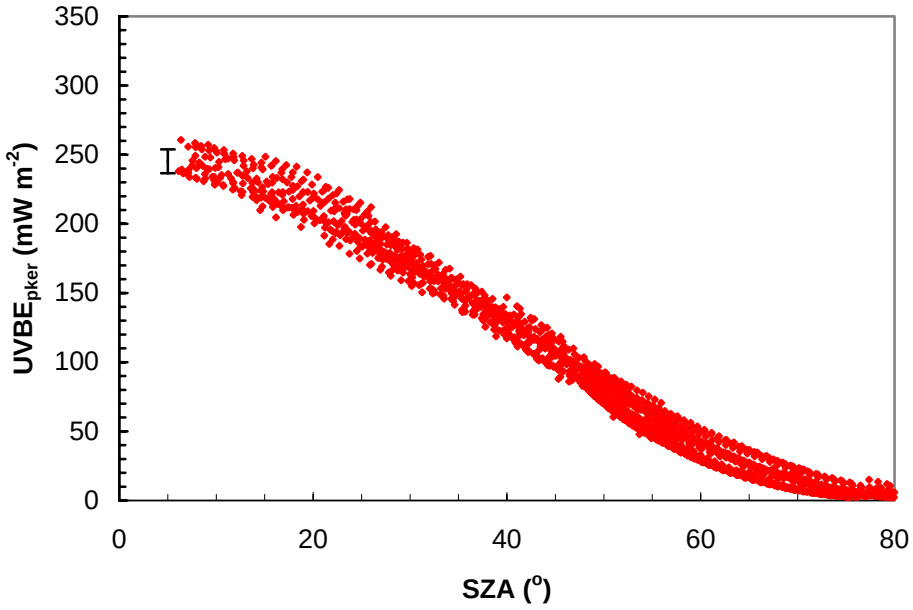

(b)

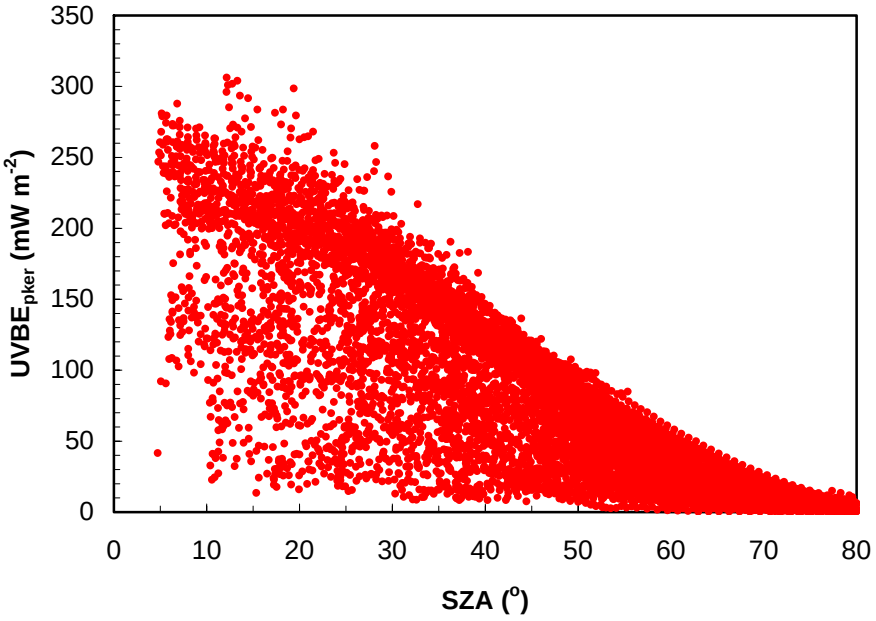

Figure 4 - The $UVBE_{pker}$ for (a) cloud free conditions and (b) all sky conditions as a function of SZA. The error bar shown in part (a) represents the 95th percentile of the cloud free cases.

(a)

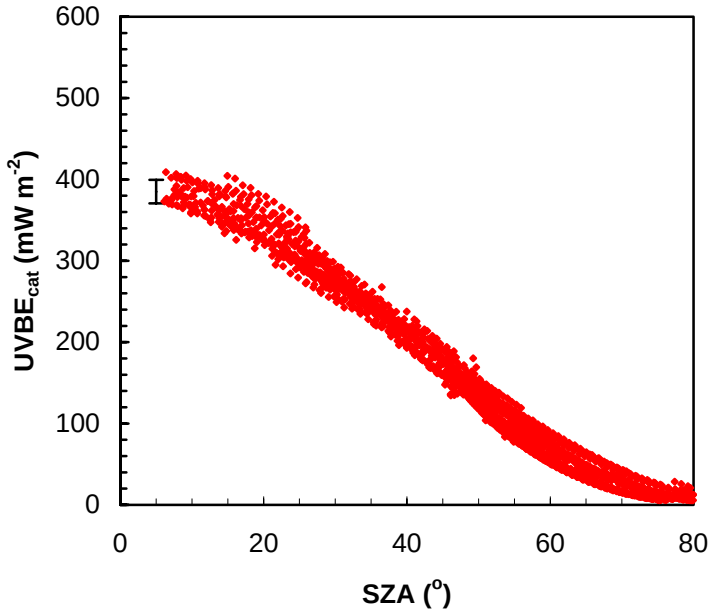

(b)

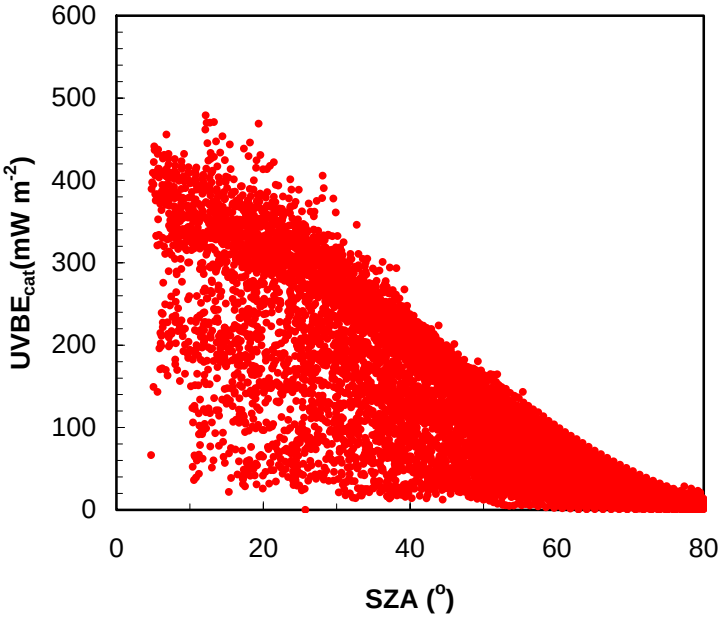

Figure 5 - The $UVBE_{cat}$ for (a) cloud free conditions and (b) all sky conditions as a function of SZA. The error bar shown in part (a) represents the 95th percentile of the cloud free cases.

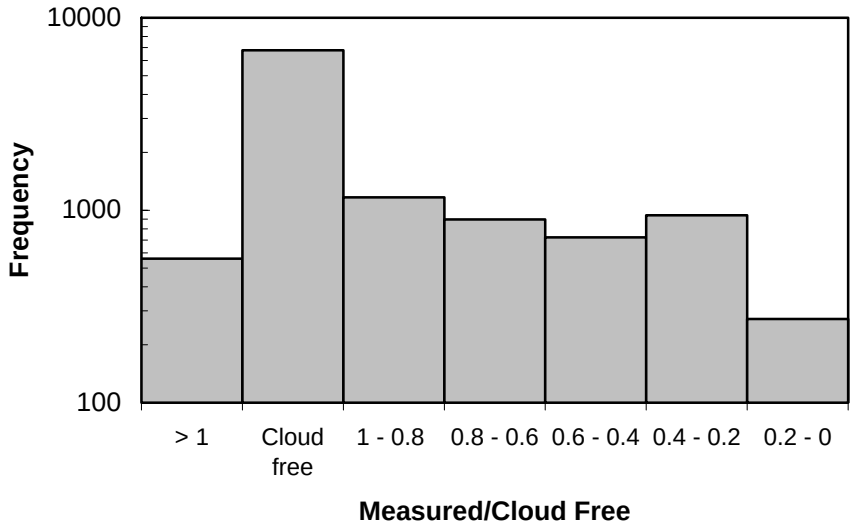

Figure 6 – Percentages within each range of the measured/cloud free values for $UVBE_{cat}$. The cloud free column is the percentage of values within ±23.1 mW m^{-2} (95^{th} percentile) of the cloud free regression curve. The > 1 column is the percentage of values higher than the cloud free regression curve at the appropriate SZA plus the 95^{th} percentile. The other columns are the percentages less than the cloud free regression curve at the appropriate SZA minus the 95^{th} percentile.

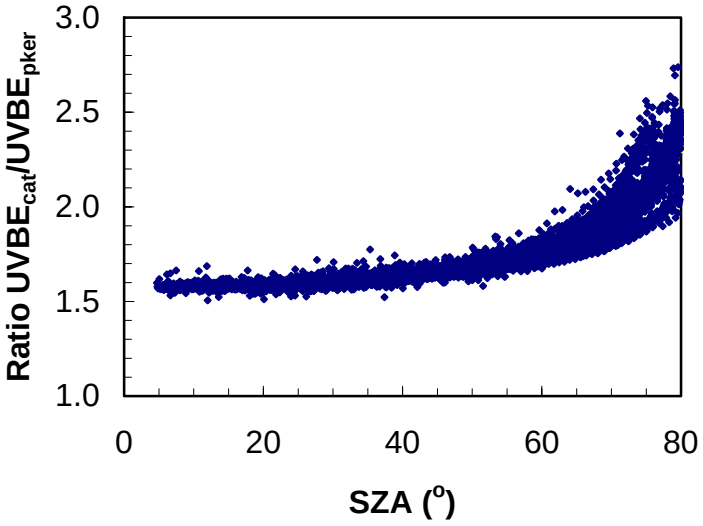

Figure 7 – Ratio of the UVBE$_{cat}$ to UVBE$_{pker}$ irradiances for all sky conditions.

(a)

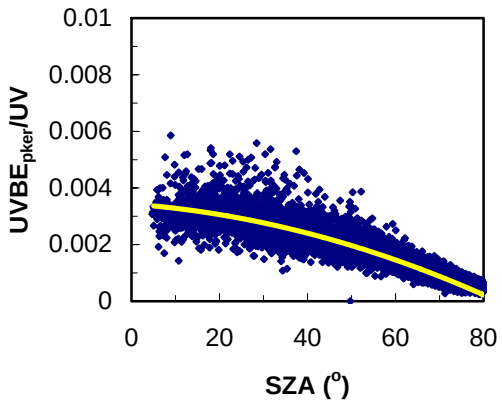

(b)

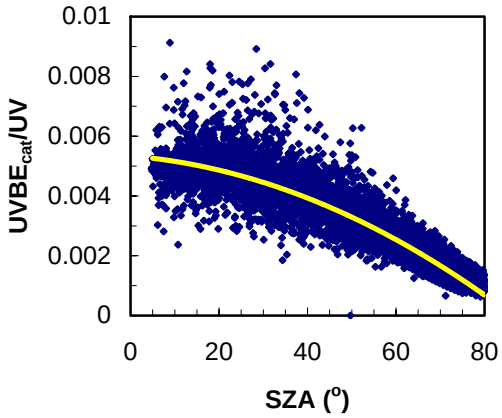

Figure 8 – Ratio of the biologically effective UV to the unweighted UV for (a) photokeratitis and (b) cataracts and the fitted regression curves.